Clay Minerals (2003) **38**, 339–352

Rythmic changes in crystal chemistry of trioctahedral Cr-chlorites and Cr entrapment: a SEM, EM and Raman study

A. C. PRIETO[1,*], M.-C. BOIRON[2], M. CATHELINEAU[2], R. MOSSER-RUCK[2], J. A. LOPEZ[3] AND C. GARCÍA[1]

[1] *Departamento de Física de la Materia Condensada, Cristalografía y Mineralogía, Universidad de Valladolid, 47011 Valladolid, Spain,* [2] *UMR CNRS G2R 7566 and CREGU, BP23, 54501 Vandoeuvre les Nancy Cedex, France, and* [3] *Departamento de Cristalografía y Mineralogía, Universidad Complutense, 28040 Madrid, Spain*

(*Received 28 January 2002; revised 26 May 2003*)

ABSTRACT: Back-scattered scanning electron microscopy (SEM) images of Cr-chlorite crystals from Erzerum (Turkey) reveal that the crystals are chemically inhomogeneous and display complex but well defined crystal zoning characterized by growth bands with contrasting chemical features. The chemical zoning has been investigated at the micron scale using an integrated approach, combining BSEM images, *in situ* chemical analysis by electron microprobe and Raman spectroscopy. Enrichment in Cr, due to octahedral Al substitution, reaches up to 0.7 atoms per half formula, especially in bands where the Mg content is depleted. These substitutions are also depicted at the micron scale on Raman spectra by changes in the ν(OH) band intensities and positions that correlate with the Cr content. The Cr-enrichment occurs thus during specific stages of crystal growth, probably in response to changes in the fluid chemistry controlling the relative availability of Cr, Mg and Al in solution.

KEYWORDS: chlorite, Cr, electron microprobe, Raman spectroscopy, SEM.

Entrapment of metals in sheet silicates has been studied extensively in a variety of examples (mostly micas), especially from the point of view of the identification of the metal location in the crystal structure, and the nature of the main cation substitution. In clays, the distribution of metals at the scale of the crystal is difficult to study because most particles are small in size, and metals are present in small amounts, frequently adsorbed on the particle surface. In some cases, however, the quality of the crystal is such that it is easier to study the distribution of the metal at the scale of growth bands, typically at the micron (to tens of microns) scale. In the case of trioctahedral chlorites, the distribution of metals such as Fe and Mn is generally investigated statistically on populations of particles, but is difficult to map due to the size of the particles. The case of the Cr-rich chlorites, which occur as mm-sized mono-crystals is rather exceptional. Crystals from Kop Krom Mine, in the Kop Daglari area, Erzerum (Turkey) are well known for their intense purple to violet colour and their euhedral crystals with perfect 001 cleavage. These chlorites formed during the uplift and subsequent alteration of Alpine podiform chromites from the Northern ophiolite belt (Billor & Gibb, 2002). Preliminary SEM examination using back scattered electron images of Cr-chlorite crystals revealed that they are inhomogeneous and display complex crystal zoning characterized by growth bands (a few to 100 μm wide) with contrasting chemical features.

* E-mail: prieto@fmc.uva.es
DOI: 10.1180/0009855033830100

The Al-Cr substitution in Cr-chlorite was studied previously in bulk powder samples and it was shown that Cr is not present in the tetrahedral site but occupies the interlayer sheet in the *M*(4) position (Phillips *et al.*, 1980). Little is known, however, of the three-dimensional location of the metal concentrations at the crystal scale, especially the Cr enrichment distribution and the range of Cr contents at the micrometer scale. Although the relationships between Cr content and the bulk chemical features of the Cr-rich growth bands are generally not reported, such data can help in the understanding of the physical conditions controlling the metal entrapment in the lattice, during the crystal growth. The main objectives of this work were thus the determination of: (1) the range of Cr substitution in Cr-chlorites; (2) the relationships between the Cr substitution and other substitutions (Mg-Al, Si-Al); and (3) the effects of Cr content and related chemical substitutions on Raman spectra at the microscopic scale.

EXPERIMENTAL

Cr-chlorite crystals were examined by SEM (secondary and back-scattered electron modes) using an Hitachi S-2500 Fevex scanning electron microscope. Quantitative analyses were carried out using a Cameca® SX 50 electron microprobe (EM) (Nancy I University) under the following analytical conditions: 15 kV acceleration voltage, 10 s counting time, 10 nA excitation current, correction program – PAP. The following minerals were used as standards: corundum (Al), albite (Na), orthoclase (Si), hematite (Fe), apatite (Ca), $KTiPO_5$ (K), forsterite (Mg), rutile (Ti), rhodonite (Mn) and chromite (Cr). The maximum analytical error was 3% of the total.

X-ray diffraction (XRD) patterns of powders and oriented crystals were recorded with a Phillips® PW-1710 diffractometer using Cu-K_α radiation, a graphite monochromator, and automatic divergence slits. Thermal analysis involved a TGA7 Perkin Elmer® device and a differential scanning calorimetric oven, DSC 30 Mettler®, with a Tc11, TA processor. A nitrogen stream and a fixed heating rate of 10ºC/min were used. The sample mass was ~8 mg. The UV-Vis standard spectra were obtained on basal sections using an automated Phillips® PU 8620 spectrometer. The measurement range was 325–1100 nm. The spectra were fitted using commercial Origin® software.

The micro-Raman spectra were recorded on a DILOR® X-Y Raman spectrometer using a 512 intensified photodiode array multichannel detector. The excitation radiation at 488.0 or 514.5 nm was provided by an Ar^+ laser (2020-05 model from Spectraphysics®). The Cr-bearing chlorite was analysed in back-scattering geometry with the laser either perpendicular or parallel to the (001) basal planes in the microscopic mode using an Olympus® BH2 microscope equipped with a Nomarski® optical system and a 100× objective (numerical aperture 0.95).

Raman profiles were obtained, recording the spectra every 50 μm along a scan line 450 μm long in crystal I. This line was also analysed using the EM. The diameter of the laser beam at the focal plane is diffraction limited according to the Rayleigh criterion (D = 1.22 λ/NA); where λ is the laser wavelength and NA is the numerical aperture of the objective. In our standard experimental conditions the lateral resolution was better than 1 μm. The Raman peaks were fitted by a convolution of Lorentzian and Gaussian bands (LABSPEC software by DILOR®).

CHARACTERIZATION OF Cr-CHLORITE POWDER

X-ray diffraction analysis

Samples were crushed to powder (<2 μm) and oriented deposits (Tricki, 1973) prepared for X-ray analysis. The XRD patterns show that the studied chlorite is an Ia polytype, in agreement with previous data from Lister & Bailey (1967) and Bailey (1975, 1986).

Thermal behaviour

Thermogravimetric (TG) analysis results reveal that the dehydroxylation process occurs in several steps: (1) a first step (not shown in Fig. 1) between 100 and 150ºC is due to the desorption of the adsorbed water; (2) the second step between 500 and 700ºC, is associated with mass losses due to dehydroxylation of the interlayer sheet (Fig. 1); and (3) the third step between 700 and 950ºC, is probably related to the loss of two hydroxyl groups in the 2:1 octahedral sheet. These results are similar to those obtained by Nelson & Guggenheim (1991) and Bai *et al.* (1993) on the behaviour of clinochlore in high pressure-high temperature

experiments, and to those obtained with magnesium trioctahedral chlorites (Prieto *et al.*, 1991a). The total mass losses obtained using a mono-crystal suggest that four molecules of water are lost per half unit cell in good agreement with theoretical data (Table 1). Dehydroxylation temperatures obtained using powders are lower than those measured with the mono-crystal. This is probably due to the Fe oxidation produced during the crystal crushing (Prieto *et al.*, 1991a, 1993).

The water-loss processes are better understood using the thermogravimetric derivative (DTG) curve, especially when comparing the data obtained on Cr-chlorite with those previously reported for Mg-(Fe) trioctahedral chlorite (Prieto *et al.*, 1991a), displaying 0.442 Fe atoms per formula unit (a.p.f.u.). Two dehydration steps are observed (Fig. 1): (1) the first one at 613ºC, a higher temperature than for the Mg(Fe) chlorite, with a mass loss of 7.1% corresponding to 2.2 H_2O, and arising from OH-Mg and OH-R(II), in the interlayer sheet; and (2) 798ºC, a lower temperature than the corresponding one in Mg(Fe) chlorite, with a mass loss of 4.56% equivalent to 1.5 H_2O molecules corresponding to the other OH-trivalent cations (Cr (III) or Al (III) bonds. Run products identified by XRD are forsterite, chromite and hercynite.

TABLE 1. Data of dehydroxylation processes of the Erzerum Cr-chlorite using the TG and DTG curves. The experimental mass loss were obtained using a mono-crystal.

Dehydroxylation	Powder		Theoretical
	Wt.%	ºC	Wt.%
Interlayer sheet	7.01	613	9.49
2:1 Octahedral sheet	4.56	798	3.16
Total	11.57		12.64

The experimental mass loss in the monocrystal was 12.45%.

Ultraviolet-visible absorption

The UV-visible spectrum shows five absorption bands located at 401, 550, 733, 891 and 1020 nm (Fig. 2). Two intense bands, located at 401 and 550 nm are assigned to Cr(III) in octahedral coordination. The corresponding electronic transitions are those observed in other inorganic compounds and are attributed to $4A_{2g} \rightarrow 4T_{2g}$ (F) of Cr(III) $(OH,O)_6$ and $4A_{2g} \rightarrow 4T_{1g}$ (F) of Cr(III) $(OH,O)_6$, respectively (Duffy, 1990). The minor band located at 733 nm could be assigned to exchange-coupled Fe(II)-Fe(III) pairs. The ^{VI}Fe(II) corresponds to broad bands at 891 and 1020 nm, (Fe(II)-Fe(III) in the octahedral site) (Bakhtin, 1985). The absorption band located at 401 nm (24.000 cm^{-1}) is responsible for the pink-violet colour of the sample. The band located at 550.2 nm corresponds to an electronic transition at 18.175 cm^{-1} (see below for further discussion of this band).

In conclusion, the Cr-chlorite studied has features similar to those of Mg-chlorite, the Cr-content modifying slightly the bulk properties. The main

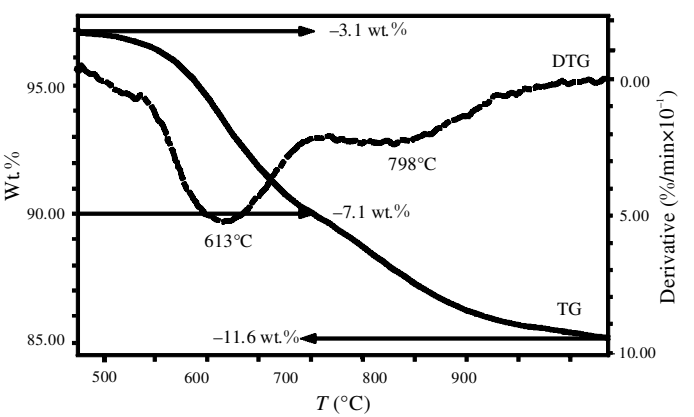

FIG. 1. Thermogravimetric (TG) and differential thermogravimetric (DTG) analysis curves of the Erzerum Cr-chlorite. The arrows indicate the weight losses at specific temperatures.

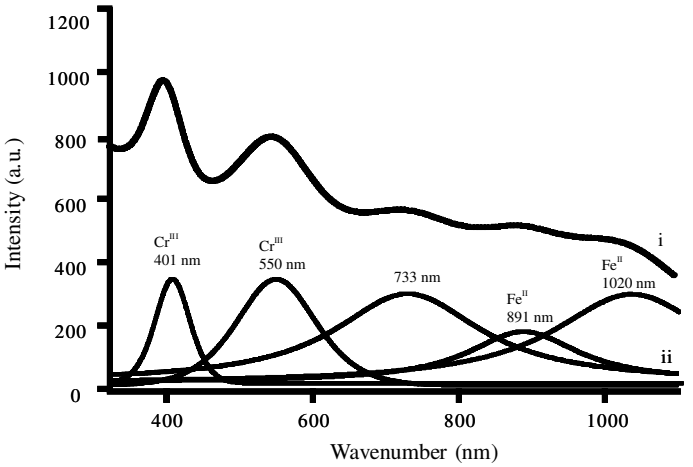

FIG. 2. UV-visible spectra of the Erzerum Cr-chlorite in the 325–1100 nm spectral range, [(i) global spectrum fitted by Fourier series; (ii) resolved components]. a.u.: arbitrary units.

difference is that found by UV-visible absorption, as shown above.

IN SITU CHARACTERIZATION

Cation distribution in Cr-bearing bands

The BSEM imaging which is able to reveal differences in the average atomic number (Z) has shown that crystals exhibit complex chemical zoning. The zoning is rhythmic, and appears on back-scattered images as alternating dark and light zones (Fig. 3). Light zones are mostly observed in the inner growth zones of the crystals, but exceptions are found, as each crystal does not display the full succession of growth zones.

Systematic analyses (3 μm step size) on two crystals (e.g. Fig. 3) showed Cr concentrations from 3.32 to 6.5% in the zones displaying higher Z (light zones in the BSE images) and corresponding to atomic Cr contents from 0.65 to 0.37 (atoms per half formula unit), respectively. A large number of analytical points was obtained (435 analyses), a selection of which came from one profile (crystal I) and is given in Table 2 (one analysis over a segment of 12 μm).

A mean structural formula, on the basis of 14 oxygen atoms, was calculated over 435 analyses (crystals I and II), considering all Fe to be divalent, as is generally the case for chlorite. The presence of trivalent Fe replacing other trivalent cations (Al or Cr) in their respective locations cannot, however, be ruled out, as indicated in the section on UV-visible data.

$$^{VI}\{Mg_{5.13(\pm 0.12)}Cr_{0.55(\pm 0.12)}Al_{0.21(\pm 0.12)}Fe(II)_{0.09(\pm 0.03)}\square_{0.02(\pm 0.05)}\}$$

$$^{IV}\{Si_{3.26(\pm 0.04)}Al_{0.74(\pm 0.04)}\}O_{10}(OH)_8$$

($\square$ = octahedral vacancy)

The Si content in the tetrahedral site, and consequently the ^{IV}Al content are remarkably constant whatever the growth bands considered, enriched or not in Cr. Line scans show that the Cr content increases with decreasing ^{VI}Al (Fig. 4), consistent with the hypothesis of an Al-by-Cr substitution. The ^{VI}Al *vs.* Cr diagram (Fig. 5) also shows that ^{VI}Al is roughly anti-correlated with Cr when considering the whole dataset, following a near 1:1 Al-Cr substitution, already defined for Cr-chlorite by Phillips *et al.* (1980). The trends are not, however, strictly parallel to the 1:1 line, as in some growth bands the ^{VI}Al content varies by 0.4 atoms at sub-constant or slightly increasing Cr contents. In addition, the trend for crystal I is shifted slightly to higher values of the sum ^{VI}Al + Cr (mean value of 0.78 in crystal I and 0.73 in crystal II) due to a difference in the octahedral Mg content which is slightly smaller in crystal I than in crystal II. As a consequence, the overall consideration of several growth bands and crystals (I and II in Fig. 5) shows that the simple Al-Cr substitution cannot be shown easily by a simple ^{VI}Al-Cr binary plot. The reason is that ^{VI}Al content is dependent

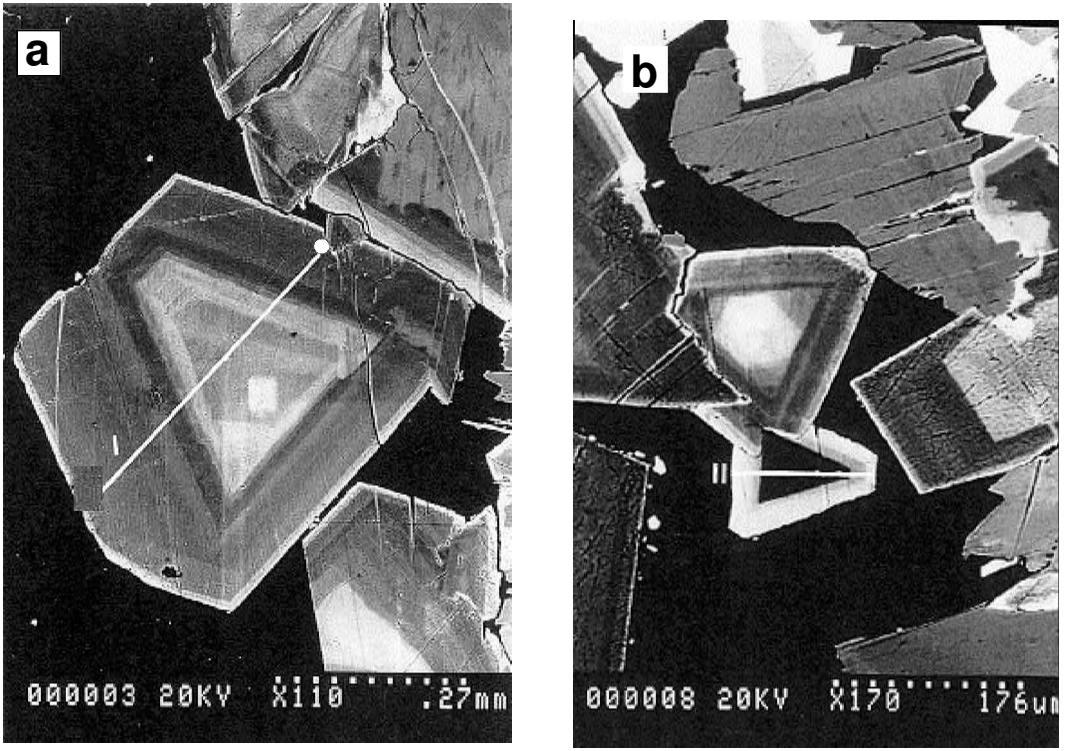

FIG. 3. BSEM images of the Erzerum Cr-chlorite crystals (a: crystal I, b: crystal II) with an indication of the electron microprobe scanning lines. Analyses were carried out every 3 μm. The dot indicates the beginning of the scanning-line in crystal I.

on three main substitutions: the Tschermak substitution, the substitution among the trivalent cations of the octahedral site, and in between divalent and trivalent cations from the octahedral site. To determine more precisely the nature of the exchange reaction, we have defined the variables x, y and z from the structural formula and correlated the substitution linearly:

$$^{IV}\{Si_{(3+x)}Al_{(1-x)}\}\,^{VI}\{[Mg,Fe(II)]_{(5+x)}[Cr,Al]_{(1-x)}\} \quad (1)$$

Substitution 1 describes the exchange between divalent and trivalent cations in the octahedral sites to satisfy the charge difference introduced by the Si-Al substitution in the tetrahedral site (Tschermak substitution). A slight imbalance between the octahedral (^{VI}Al + Cr) and tetrahedral charge (^{IV}Al) indicates that further substitutions need to be considered. Thus, in addition to substitution 1, we correlate the octahedral vacancy by:

$$^{VI}\{[Mg,Fe(II)]_{(5-3z/2)}[Cr,Al]_{(1+z)}(\square_{z/2})\} \quad (2)$$

Better correlations are obtained when only two substitutions are considered together: (1) a Tschermak substitution (equation 1) which is depicted by the positive correlation between Mg and Si, when the Si is corrected from substitution 2, e.g. the relationships Mg = (Si-1-3vac) + 3 is satisfied (correlation coefficient = 0.91); and (2) a negative correlation between ^{VI}Al and Cr when corrected from the Si content and vacancy variations (equations 1 and 2, e.g. ^{VI}Al = (4-Si+2vac)-Cr, with a correlation of 0.98). Thus, Al exchanges for one Cr in the octahedral site as follows:

$$^{VI}\{[Cr_{1-y},Al_y]\} \quad (3)$$

but is dependent on x, y and z values as indicated below by the ideal formula:

$$^{IV}\{Si_{(3+x)}Al_{(1-x)}\}\,^{VI}\{[Cr_{(1-x-y+z)},Al]_y[Mg,(Fe(II)]_{(5+x-3z/2)}[\square_{z/2}]\}$$

Because each growth band and crystal is characterized by specific values of x, y and z, no

TABLE 2. Selected structural formula (in atoms per half formula) from the traverse-line carried out on crystal I. Values correspond to analytical points (one point over 4, e.g. every 12 μm). Ca, Na, K and Ti are below detection limit. (□: vacancy)

Nº	Si	^{IV}Al	^{VI}Al	Fe	Mg	Cr	□
8	3.26	0.74	0.33	0.09	5.15	0.40	0.02
12	3.27	0.73	0.35	0.08	5.17	0.39	0.01
16	3.30	0.70	0.35	0.08	5.14	0.40	0.04
20	3.25	0.75	0.36	0.07	5.13	0.41	0.03
24	3.26	0.74	0.36	0.08	5.18	0.38	0.01
28	3.31	0.69	0.34	0.07	5.13	0.42	0.04
32	3.21	0.79	0.26	0.06	5.13	0.55	0.01
36	3.22	0.78	0.19	0.06	5.07	0.64	0.04
40	3.26	0.74	0.13	0.06	5.11	0.66	0.03
44	3.27	0.73	0.24	0.07	4.97	0.63	0.09
48	3.25	0.75	0.23	0.05	5.06	0.61	0.05
52	3.27	0.73	0.21	0.08	5.07	0.60	0.05
56	3.29	0.71	0.19	0.08	5.09	0.59	0.06
60	3.24	0.76	0.25	0.08	5.00	0.61	0.06
64	3.25	0.75	0.28	0.07	5.00	0.58	0.07
68	3.29	0.71	0.16	0.06	5.08	0.64	0.05
72	3.32	0.68	0.24	0.05	5.01	0.61	0.09
76	3.27	0.73	0.33	0.06	5.02	0.52	0.07
80	3.25	0.75	0.43	0.05	5.14	0.35	0.03
84	3.27	0.73	0.35	0.06	5.20	0.38	0.01
88	3.28	0.72	0.30	0.07	5.17	0.44	0.02
92	3.31	0.69	0.37	0.06	5.13	0.39	0.05
96	3.24	0.76	0.34	0.10	5.15	0.40	0.02
100	3.28	0.72	0.37	0.08	5.11	0.41	0.04
104	3.33	0.67	0.36	0.09	5.13	0.38	0.05
108	3.30	0.70	0.40	0.08	5.07	0.39	0.06
112	3.31	0.69	0.38	0.09	5.07	0.40	0.06
116	3.29	0.71	0.35	0.09	5.13	0.40	0.03
120	3.32	0.68	0.31	0.10	5.11	0.43	0.05
124	3.29	0.71	0.31	0.07	5.12	0.44	0.05
128	3.33	0.67	0.33	0.10	5.06	0.45	0.06

direct relationships are found therefore from the overall consideration of the analyses as a consequence of the combined effects of the three substitutions.

Enrichment in Cr up to 0.7 atoms per half formula (a.p.h.f.) in crystals I and II is found in some growth bands which are depleted in octahedral Al (Cr-Al substitution) but also in Mg, at nearly constant Fe and tetrahedral Al content. In a Cr-rich zone, at nearly constant Cr content, a local negative correlation between octahedral Al and Mg is shown clearly by the profile from Fig. 4, within second-order growth bands (e.g. growth band between the dotted vertical lines). In Cr-poor growth bands, Cr is ~0.4, and Mg is increased from 0.1 up to 0.2 in comparison with the Mg-depleted second-order bands.

Raman spectroscopy

Si-Al substitutions in the tetrahedral, and Cr-Al, Fe-Mg in octahedral 2:1 and interlayer sheets of trioctahedral chlorites produce variations in both the layer thickness and the O–OH bond length (Shirozu, 1980, 1985). The effect is caused by an increase in the net negative charge of the 2:1 layer and the octahedral cations in the interlayer. Previous studies (Prieto *et al.*, 1991a,b) of trioctahedral Fe and Mg end-member chlorites emphasized the strong correlation between macroscopic characteristics (e.g. structural, spectroscopic) and substitutions in cation lattice sites. Similar investigations have been carried out on other end-members of the chlorite series (Shirozu *et al.*, 1975). However, the concentration range of Cr contents in Cr-chlorite is lower than the Fe concentration range in Fe-Mg chlorite series.

The interpretation and assignment of the IR-Raman bands are based on Ishii *et al.* (1967) and Farmer (1974). Vibrational modes may be assigned in a first approximation as described in Table 3. Besides, complementary data are obtained by polarizing the electric field E of the incident radiation parallel or perpendicular to the (001) basal plane of the crystal. The spectrum of Cr-chlorites is separated in five spectral ranges for discussion: 3700–3630 cm^{-1}, 3630–3300 cm^{-1}, 1500–800 cm^{-1}, 800–600 cm^{-1} and <600 cm^{-1}. Stretching vibrations of hydroxyl groups, ν(OH), produce intense and well defined bands in the 3300–3700 cm^{-1} spectral range. The number of OH-related peaks, their positions, and their relative intensities vary from mineral to mineral and are controlled by the type and number of crystallographically equivalent OH-group sites, the type of cations bonded to the OH site and the cation occupancy probabilities (Wang *et al.*, 2002).

3700–3630 cm^{-1} spectral range. The band observed near 3680 cm^{-1} is assigned to ν(OH) in the 2:1 layer. This band is similar to those reported for talc (Serratosa & Viñas, 1964; Hayashi & Oinuma, 1965, 1967; Prieto *et al.*, 1990, 1991b). This band appears controlled by the average cation content within the 2:1 layer. The high frequency of this vibration indicates that the hydroxyl group does not participate in hydrogen bonding. The intensity of the band is dependent on the plane of scattering

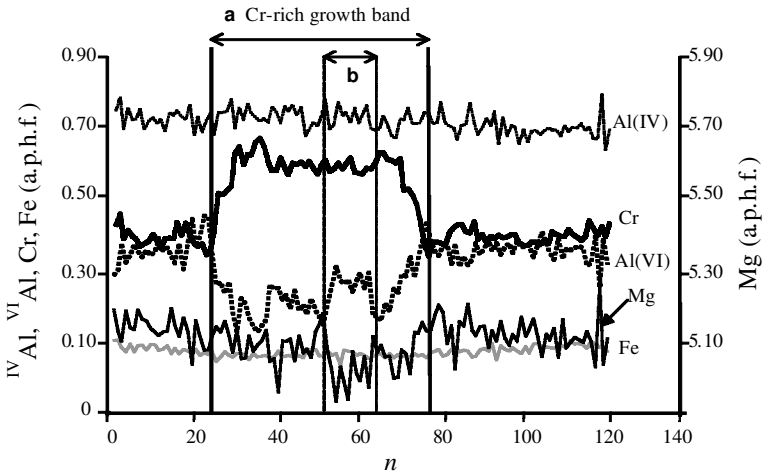

FIG. 4. ^{IV}Al, ^{VI}Al, Fe, Cr and Mg contents (atoms per half formula: a.p.h.f.) determined from quantitative electron microprobe analysis (crystal I) along the profile shown in Fig. 3a. *n* refers to analysis number, each analytical point being 3 μm from the next. Vertical lines indicate the location of a Cr-rich growth band (a), and vertical dotted lines the location of a secondary order growth band (b) showing a depletion in Mg correlating to an increase in octahedral Al.

laser polarization. The spectra show that the intensity of the band with E parallel to the (001) crystal plane is greater than that with E perpendicular to the (001) plane (Fig. 6).

This Raman band shows a shoulder in the low-frequency side. By deconvolution of the the band, a second peak at 3663 cm^{-1} is resolved. The two peaks (3680 cm^{-1} and 3663 cm^{-1}) are associated

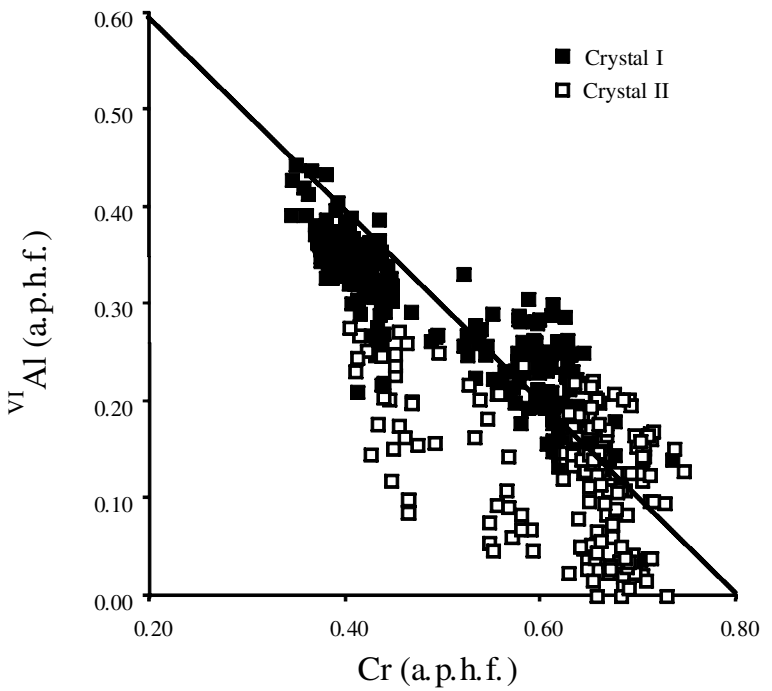

FIG. 5. ^{VI}Al *vs*. Cr diagram for the Erzerum Cr-chlorite crystals I and II (a.p.h.f. : atoms per half formula).

TABLE 3. Micro-Raman data for Erzerum Cr-chlorite (Turkey). Electric field E of the incident radiation (A) parallel and (B) perpendicular to the (001) basal plane of the crystal.

Micro-Raman (cm^{-1}) A	B	Assignment
86 vw	87 vw	ν_6F_{2u} MO_6
101 vw	100 vw	ν_5F_{2g} MO_6
199 w	199 vs	ν_1A_{1g} MO_6
	238 w	
285 m	285 m	(E_1^3) ν (T_2O_5)
328 vw	322 vw	
357 m	354 m	$MO_4(OH)_2$ 2:1
391 w	387 w	skeletal modes
428 w	429 sh	Librat. (OH)
462 w	464 m	(E_2^2) ν (T_2O_5)
542 vs	542 vs	(E_1^2) ν (T_2O_5)
	655 sh	Librat. (OH)
683 vs	680 s	(A_1^2),(E_2^1) ν (T_2O_5)
1058 w	1058 m	(E_1^1) ν (T_2O_5)
1092 vw	1092 sh	
1216 vw		
1224 vw		(E_1^2) + (A_1^2), (E_2^1)
1252 vw		
1297 vw		
	3440 s	ν (OH) (OH...O)SiSi
	3547 vs	ν (OH) (OH ... O)SiAl
3681vs	3681 m	ν (OH) 2:1

vs: very strong; s: strong; m: medium; w: weak;

with $\nu_s+\nu_{as}$ (OH)-3Mg and $\nu_s+\nu_{as}$ (OH)-Mg_2,R(II), respectively, according to the notation adopted for IR spectra, Farmer (1974). This behaviour was also reported for magnesian chlorites with very low Fe concentrations (Prieto *et al.*, 1991b). This suggests that the hydroxyl groups are aligned transversally to the (001) plane.

3630–3300 cm^{-1} spectral range. The two bands observed in this range are less intense and broader (~150–200 cm^{-1} full width at half maximum) for E perpendicular to the (001) plane (Fig. 6).

These bands almost vanish for E parallel to the (001) basal plane. The bands at 3592 cm^{-1} (E//(001)) and 3600 cm^{-1} (E//(001)) are assigned to ν(OH) in the interlayer (SiSi)(O...OH). The band at 3440 cm^{-1} is observed only for E parallel to (001) and was assigned to ν(OH) in the interlayer (SiAl)(O...HO) (Shirozu, 1980, 1985).

Lower-frequency bands indicate that the corresponding hydroxyl groups were involved in hydrogen bonds. Therefore, most hydrogen bonds assigned to (SiSi)(O...HO) were roughly perpendicular to the basal plane. Polarization measurements confirmed this. The 3592 cm^{-1} band is very intense with E perpendicular to the (001) plane and very weak with E parallel to the (001) plane. Instead of this, the intensities of the bands near 3440 cm^{-1}, assigned to (SiAl)(O...HO) are very low, regardless of the orientation of the electric field.

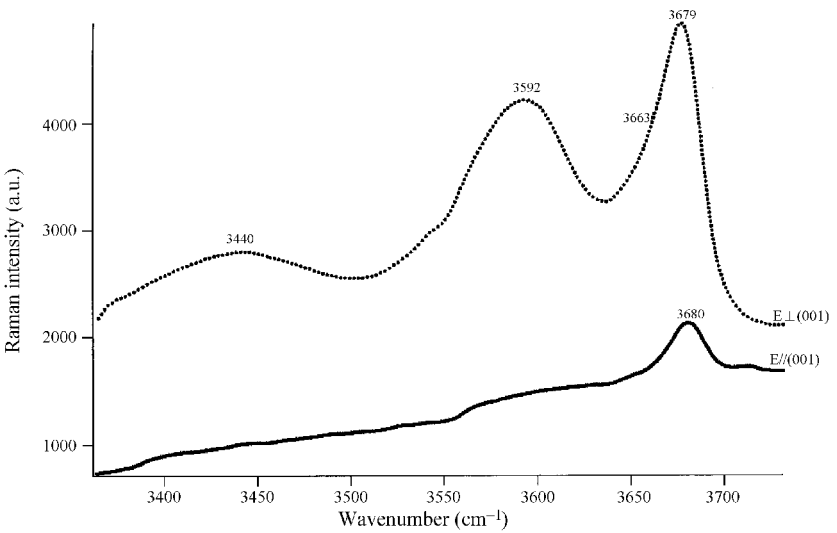

FIG. 6. Micro-Raman spectra of the Erzerum Cr-chlorite in the 3375–3725 cm^{-1} spectral range recorded for two different scattering geometries.

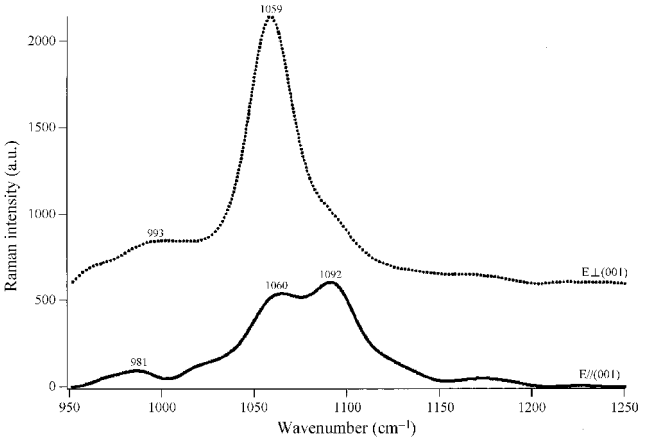

FIG. 7. Micro-Raman spectra of the Erzerum Cr-chlorite in the 950–1250 cm^{-1} spectral range for two different scattering geometries.

1500–800 cm^{-1} spectral range. The Raman peaks in the spectral region 1500–800 cm^{-1} arise from the stretching mode of the $(Si_2O_5)_n$ groups in SiO_4 tetrahedra and to the librational movements of H_2O. Vibrations of the tetrahedral sheet originate in the ditrigonal rings (Si_2O_5) having a maximum symmetry C_{6v} (Ishii *et al.*, 1967). Normal vibrational modes of this group were assigned to the following symmetry species: $2A_1 + 3B_1 + 1B_2 + 3E_1 + 3E_2$. E_1 and E_2 are Raman active and A_1 and E_1 are IR active. Frequency calculations were reported by Vedder (1964), Ishii *et al.* (1967) and Pampuch & Ptak (1968). Substitution of Si and Al induced a loss of symmetry of the $(Si,Al)_2O_5$ groups from C_{6v} to C_s. Nevertheless, the assumption of C_{6v} symmetry remains reliable for band assignments. The bands at 1059–1092 cm^{-1} are weak in the micro-Raman spectra and strongly polarized with an intensity maximum if the electric field of the laser beam is perpendicular to the basal plane. Therefore, this band corresponds to the (Si,Al)–O (apical) bonds. The frequency is shifted slightly towards lower values with increasing ^{IV}Al. This effect is shown in Fig. 7 as a function of the polarization of the incident electric field. In the case of E parallel to the basal plane, a shoulder appears in the spectrum for each band, resulting from two different environments for the tetrahedral position.

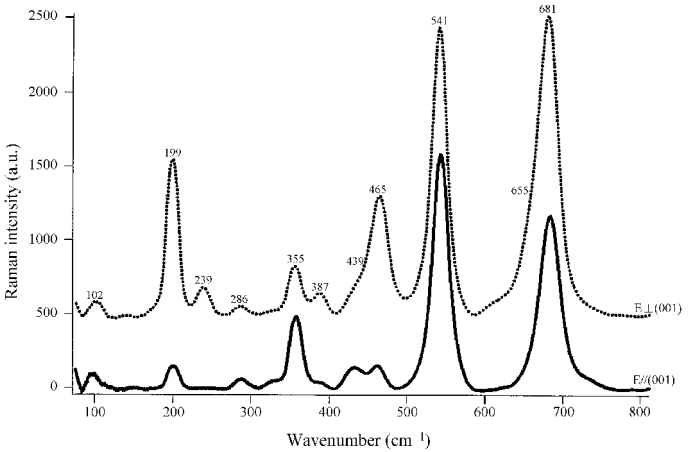

FIG. 8. Micro-Raman spectra of Erzerum Cr-chlorite in the 75–800 cm^{-1} spectral range for two different scattering geometries.

800–600 cm^{-1} spectral range. The Raman peaks in this spectral range are contributed by the vibrational modes of Si–O–Si bonds, which connect the SiO_4 tetrahedra. The micro-Raman spectra (Fig. 8) exhibit bands at 681 and 655 cm^{-1}. Most trioctahedral chlorites show a strong peak in this spectral range. Hydrogen substitution by deuterium demonstrated that these bands contain a contribution of OH vibrations (Shirozu & Ishida, 1982; Shirozu, 1985). The band at 681 cm^{-1} was assigned to a vibrational mode (A_1^2, E_2^1) ν(Si,Al_2O_5) combined with OH vibrations. Therefore, this vibration was strongly dependent on the composition of the octahedral sheet interlayer and the 2:1 layer (Ishii *et al.*, 1967; Shirozu & Ishida, 1982; Shirozu, 1985). The tetrahedral substitutions (Si^{4+}-Al^{3+}) and the octahedral sheet substitution of Mg^{2+} for Al^{3+}, and for Fe^{2+} induce distortions in both the octahedra and the tetrahedra of the 2:1 layer, modifying the Si–O–Si bonds. Reductions of the bond lengths (Si–O–Si) ($\approx$0.05 Å) result in high-frequency shifts of 30 cm^{-1} (Wang *et al.*, 2002). Consequently, the frequency of the peak at 681 cm^{-1} suggests a small amount of R(II), R(III) substitution in the 2:1 octahedral sheet.

<600 cm^{-1} spectral range. The Raman peaks in this spectral range arise from the translational motions of oxygens, OH groups and cations in either octahedral sites or interlayer sites to the SiO_4 groups in the tetrahedral sheets (transitional and librational modes are included) (Wang & Valentine, 2002).

The micro-Raman spectra display a very intense band (541 cm^{-1}) and a low-intensity band at 465 cm^{-1} (Fig. 8). They are attributed to fundamental modes E_1^2 and E_2^1 $\nu(T_2O_5)$. The E_2^1 $\nu(T_2O_5)$ band is very intense with E//(001). Weak Raman bands are observed near 400 cm^{-1}. They are assigned to a combination of vibration of ionic and molecular groups and correspond to skeletal modes, e.g. the internal movement of metal oxygen coordination. The peak around 355 cm^{-1} was assigned to internal movements of octahedral sheets. Such a band has also been reported in talc (Blaha & Rosasco, 1978; Rosasco & Blaha, 1980). This band is characteristic of Mg–O bonds.

A weak intensity band at 286 cm^{-1} is assigned by Ishii *et al.* (1967) and Shirozu (1985) to tetrahedral movements with E_1^3 symmetry. The intense peak at 199 cm^{-1} is assigned to symmetric stretching of the octahedral site and shows an intensity dependence with orientation. This band does not depend on the Si-Al substitution but was strongly dependent on Fe-Mg-Al-Cr substitution.

The Raman spectrum of this Cr-chlorite appears similar to that of clinochlore, with a chemical composition [$(Si_{2.80}Al_{1.20})(Mg_{4.35}Al_{1.20}Fe_{0.43})O_{10}(OH)_8$], studied in a previous report (Prieto *et al.*, 1990, 1991b). However, both mineral species present differences regarding the intensity ratios of the bands in the spectral range assigned to ν(OH) located within the 2:1 layer and in the region of the ν(SiSi)O...OH band. As Cr is substituted for Al, it is reasonable to attribute changes in this band to changes in the Cr content.

Relationships with Cr-Al substitution

Micro-Raman investigations have been carried out on individual crystals with a special emphasis on the zones displaying the highest contrast in Cr contents. We attempted to correlate the crystal-chemistry Cr/Al zoning to changes in the dynamic vibrational features on the same profile studied for crystal-chemistry (crystal I, Fig. 3). Raman spectra (3450–3750 cm^{-1}, spectral range) obtained along this line are shown in Fig. 9. The Raman profile of crystal I shows a shift to the low frequencies of the stretching modes associated with ν(OH) in the octahedral sheet of the 2:1 layer in between 100 and 300 μm. Also, a change in the intensity and the line width of the band around ~3600 cm^{-1}, associated with stretching modes ν(SiSi)O...OH is observed. The shift of the bands to the lower frequencies and the change of the Raman intensities can be related to the Cr/Al concentration ratio distribution, determined by SEM-EDX in crystal I (Figs 10, 11).

The structural chemistry of the chlorite group has been reviewed by Bailey (1988). Chemical and structural studies on chlorites (Rule & Bailey, 1989; Zheng & Bailey, 1989; Welch *et al.*, 1995; Smyth *et al.*, 1997) have indicated considerable ordering of the octahedral cations. The tetrahedral sheets are each composed of equal numbers of two distinct tetrahedra, *T*1 and *T*2. The octahedral sheet in the 2:1 layer comprises two distinct octahedra, *M*1 and *M*2, with *M*1 at the origin, trans-bonded OH, and *M*2 in a general site position *cis*-bonded to OH. Similarly, the interlayer sheet includes two distinct octahedra, *M*3 and *M*4, with *M*3 in a general position and *M*4 on a inversion site; this means that there are half as many *M*4 sites per layer. The two

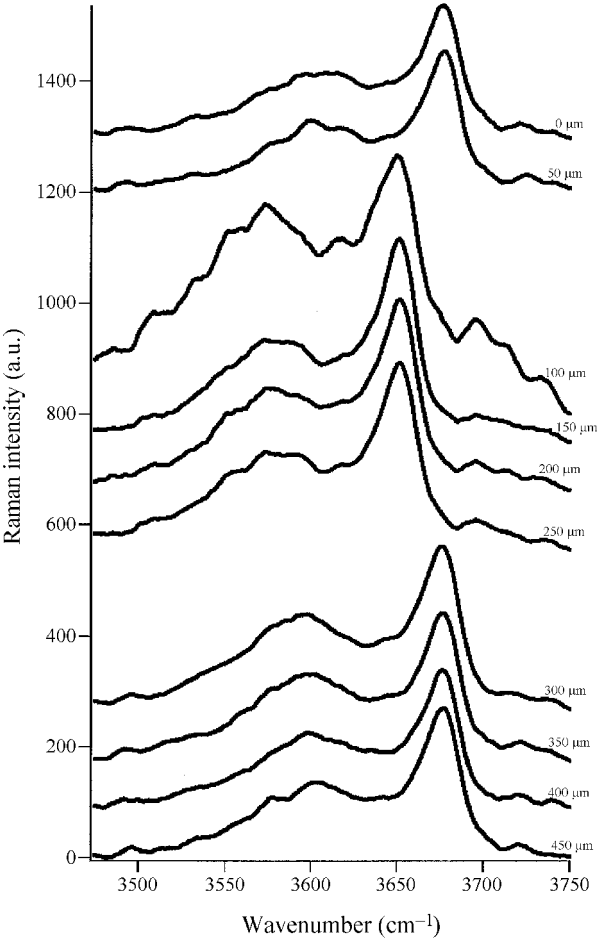

FIG. 9. Micro-Raman spectra obtained along a line crossing crystal I in the spectral range 3450 – 3750 cm^{-1}.

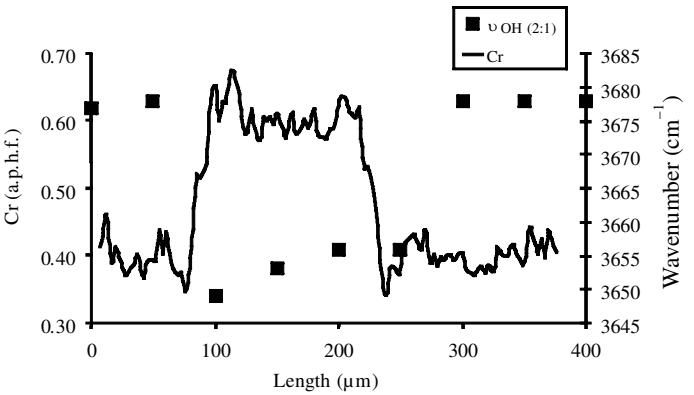

FIG. 10. Evolution of micro-Raman parameters along a scanning-line crosscutting a band enriched in Cr (crystal I). Cr content (atoms per half formula – a.p.h.f.) and the wavenumber stretching ν(OH-Mg) band *vs.* length (µm) are given.

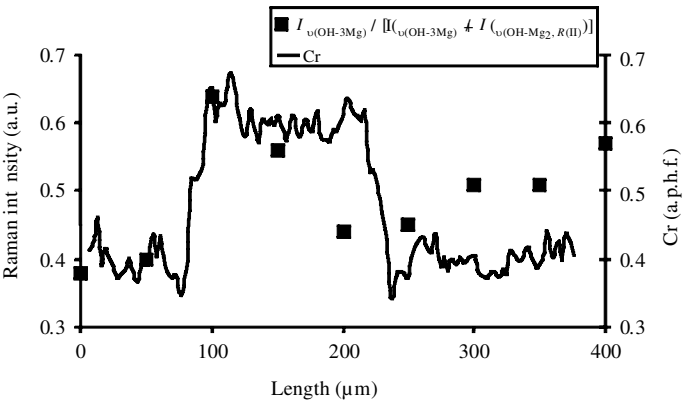

FIG. 11. Evolution of micro-Raman parameters along a traverse-line crosscutting a band enriched in Cr (crystal I). Cr content (atoms per half formula – a.p.h.f.) and ratio of stretching ν(OH) band intensities ($I_{vs+vas\ (OH)\text{-}3Mg}$/($I_{vs+vas\ (OH)\text{-}3Mg}$ + $I_{vs+vas\ (OH)\text{-}Mg_2,R(II)}$) *vs.* length (μm).

octahedra in the interlayer sheet differ considerably in volume, distortion and mean cation–oxygen distance. Trivalent cations (Al and Cr) concentrate in the interlayer sheet, creating a net positive charge to balance the net negative charge on the 2:1 layer. Furthermore, the trivalent cations tend to concentrate into the smaller *M*4 sites, which have less distortion than the *M*3 sites (Lister & Bailey, 1967; Smyth *et al.*, 1997; Phillips *et al.*, 1980).

The detailed examination of the Raman parameters (frequency, intensity) as a function of the Cr/Al substitution shows significant relationships between crystal-chemistry and dynamic vibrational features (Figs 10, 11). Spectra deconvolution was performed using a combination of Gaussian and Lorentzian functions. The integrated intensity of each band was obtained and these intensities were used to calculate data of Fig. 11.

The substitution Al^{3+}/Cr^{3+} takes place preferentially in the *M*4 octahedra of the interlayer sheet inducing strong distortions in the *M*3 octahedra. These distortions produce extension along the 001 crystal axes. This produces a compressive deformation of the 2:1 layer, along such a direction. Simultaneously, the (OH)-3Mg and (OH)-Mg_2,R(II) bonds of the *M*1 and *M*2 octahedra are elongated. This results in an anti-correlation between [Cr^{3+}] and the stretching of $\nu_s+\nu_{as}$ (OH)-3Mg and $\nu_s+\nu_{as}$ (OH)-Mg_2,R(II) along the scanning line. The Cr^{3+}-rich region in the centre of the crystal presents stretching bands $\nu_s+\nu_{as}$ (OH)-3Mg and $\nu_s+\nu_{as}$ (OH)-Mg_2, R(II) shifted to the low frequencies by 30 cm^{-1}. In consequence, the fluctuations in the intensity ratio, $I_{vs+vas\ (OH)\text{-}3Mg}$/($I_{vs+vas\ (OH)\text{-}3Mg}$ + $I_{vs+vas\ (OH)\text{-}Mg2,R(II)}$), is similar to those of the Cr^{3+} concentration along the scanning line.

SUMMARY

Cr-chlorite crystals are characterized by rhythmic compositional changes during their growth. The incorporation of Cr appears limited to relatively small concentrations, e.g. 0.72 per half formula in the case of the Erzerum chlorite due to the limitations imposed by the Cr location in the interlayer position and by mass and electric balance constraints. The presence of Cr (III) in octahedral coordination has been, for the first time, recognized by two intense bands (401 and 550 nm) in the UV-visible spectrum, and by specific changes occurring in band intensities and position on Raman spectra, making possible the identification of the main effects of Cr incorporation on vibrational features of the chlorite solid solutions.

The rhythmic Al/Cr changes among growth bands probably correspond to Cr availability in the solution during the crystal growth. The enrichment in Cr is correlated to a decrease in the octahedral Al occupancy (Cr-Al substitution) together with a depletion in Mg, at nearly constant Fe content. Therefore, the Cr-enrichment is a response to specific changes in the availability of Cr, but also of Mg and Al in solution, and is probably a marker of oscillatory fluctuations in the bulk fluid chemistry during chlorite growth.

ACKNOWLEDGMENTS

This work is dedicated to J.M. Claude who helped with the electron microprobe analyses carried out at the Service Commun d'Analyses de l'Université de Nancy I, and who died prematurely in January 1997. The authors thank A.M. Karpoff, A. Decarreau and an anonymous reviewer for comments and suggestions that helped to improve the manuscript. The sample was provided by Mr L. Perrichon.

REFERENCES

Bai T.B., Guggenheim S., Wang S.J., Rancourt D.G. & Koster van Groos A.F. (1993) Metastable phase relations in the chlorite-H_2O system. *American Mineralogist*, **78**, 1208–1216.

Bailey S.W. (1975) Cation ordering and pseudo-symmetry in layer silicates. *American Mineralogist*, **60**, 175–187.

Bailey S.W. (1986) Re-evaluation of ordering and local charge-balance in Ia chlorite. *The Canadian Mineralogist*, **24**, 649–654.

Bailey S.W. (1988) Chlorites: structures and crystal chemistry. Pp. 347–398 in: *Hydrous Phyllosilicates (exclusive of Micas)* (S.W. Bailey, editor). Reviews in Mineralogy, **19**. Mineralogical Society of America, Washington, D.C.

Bakhtin A.I. (1985) The distribution of Fe ions in chlorites. *Geokhimiya*, **10**, 1519–1523.

Billor M.Z. & Gibb F. (2002) The mineralogy and chemistry of the chromite deposits of southern (Kizilda, Hatay and Islahiye, Antep) and Tauric ophiolite belt (Pozanti-Karsanti, Adana), Turkey. *9th International Platinum Symposium*, Billings, Montana (USA).

Blaha J.J. & Rosasco G.J. (1978) Raman microprobe spectra of individual microcrystals and fibers of talc, tremolite, and related silicate minerals. *Analytical Chemistry*, **50**, 892–896.

Duffy J.A. (1990) *Bonding Energy Levels and Bands in Inorganic Solids*. Longman Scientific and Technical, Harlow, Essex, UK, 249 pp.

Farmer V.C. (1974) The layer silicates. Pp. 331–363 in: *The Infrared Spectra of Minerals* (V.C. Farmer, editor). Monograph **4**, Mineralogical Society of London.

Hayashi H. & Oinuma K. (1965) Relationship between infra-red absorption spectra in the region of 450–900 cm^{-1} and chemical composition of chlorite. *American Mineralogist*, **50**, 476–483.

Hayashi H. & Oinuma K. (1967) Si-O absorption bands near 1000 cm^{-1} and OH absorption bands of chlorites. *American Mineralogist*, **52**, 1206–1210.

Ishii M., Shimanouchi T. & Nakahira M. (1967) Far infrared absorption spectra of layer silicates. *Inorganic Chimica Acta*, **1**, 387–392.

Lister J.S. & Bailey S.W. (1967) Chlorite polytypism: IV regular two-layer structures. *American Mineralogist*, **5**, 1614–1631.

Nelson D.O. & Guggenheim S. (1991) Inferred limitations to the oxidation of iron in chlorite. A single-crystal high-temperature X-ray study. *American Mineralogist*, **76**, 1193–1200.

Pampuch R. & Ptak W. (1968) Infrared spectra of 1:1 layer silicates. *Polska Akademii Nauk. Oddizial Krakowie, Prace Mineral*, **15**, 7.

Phillips T.L., Loveless J.K. & Bailey S.W. (1980) Cr^{3+} coordination in chlorites: a structural study of ten chromian chlorites. *American Mineralogist*, **65**, 112–122.

Prieto A.C., Dubessy J., Cathelineau M. & Rull F. (1990) Estudio y caracterizacion de cloritas trioctaedricas por espectroscopia Raman e infra-Rojo. *Boletín de la Sociedad Española de Mineralogía*, **13**, 25–34.

Prieto A.C., Lobon J.M., Alia J.M., Rull F. & Martin F. (1991a) Thermal and spectroscopic analysis of natural trioctahedral chlorites. *Journal of Thermal Analysis*, **37**, 969–981.

Prieto A.C., Dubessy J. & Cathelineau M. (1991b) Structure composition relationships in trioctahedral chlorites: a vibrational spectroscopy study. *Clays and Clay Minerals*, **39**, 531–539.

Prieto A.C., Medina J., Calvo B., Alonso M., Boiron M.C. & Cathelineau M. (1993) Estudio y caracterizacion preliminar de cromo-cloritas de Erzarum (Turquia). *Boletín de la Sociedad Española de Mineralogía*, **16**, 101–102.

Rosasco G.J. & Blaha J.J. (1980) Raman microprobe spectra and vibrational mode assignments of talc. *Applied Spectroscopy*, **34**, 140–144.

Rule A.C. & Bailey S.W. (1989) Refinement of the crystal structure of a monoclinic ferroan chlinochlore. *Clays and Clay Minerals*, **35**, 129–138.

Serratosa J.M. & Viñas J.M. (1964) Infrared investigation of the OH bands in chlorites. *Nature*, **202**, 999.

Shirozu H. (1980) Cation distribution, sheet thickness, and O-OH space in trioctahedral chlorites – an X-ray and infrared study. *Mineralogical Journal*, **10**, 14–34.

Shirozu H. (1985) Infrared spectra of trioctahedral chlorites in relation to chemical composition. *Clay Science*, **6**, 167–176.

Shirozu H. & Ishida K. (1982) Infrared study of some 7 Å and 14 Å layer. *Mineralogical Journal*, **11**, 161–171.

Shirozu H., Sakasegawa T., Katsumoto N. & Oxaki M. (1975) Mg-lepto-chlorites – IR. *Clay Science*, **4**, 305–321.

Smyth J.R., Dyar M.D., May H.M., Bricker O.P. & Acker J.G. (1997) Crystal structure refinement and Mössbauer spectroscopy of an ordered, triclinic

clinochlore. *Clays and Clay Minerals*, **45**, 544–550.
Tricki R. (1973) *Mise au point d'une technique de coupes minces pour l'étude des minéraux par diffraction électronique. Minéraux argileux.* Ing. Doc. thesis University of Strasbourg, France.
Vedder W. (1964) Correlation between infrared spectrum and chemical composition of micas. *American Mineralogist*, **49**, 736–768.
Wang A. & Valentine R.B. (2002) Seeking and identifying phyllosilicates on Mars – A simulation study. *Lunar and Planetary Science XXXII*, 1370.
Wang A., Freeman J. & Kuebler K.E. (2002) Raman spectroscopy characterization of phyllosilicates. *Lunar and Planetary Science XXXIII*, 1374.
Welch M.D., Barras J. & Klinowski J. (1995) A multinuclear NMR study of clinochlore. *American Mineralogist*, **80**, 441–447.
Zheng H. & Bailey S.W. (1989) Structures of intergrown triclinic and monoclinic IIb chlorites from Kenya. *Clays and Clay Minerals*, **37**, 308–318.